4370 *Inorg. Chem.* **2010**, *49*, 4370–4382
DOI: 10.1021/ic100177n

Inorganic Chemistry
Article

An NMR and DFT Investigation on the Conformational Properties of Lanthanide(III) 1,4,7,10-Tetraazacyclododecane-1,4,7,10-tetraacetate Analogues Containing Methylenephosphonate Pendant Arms

Mihály Purgel,[†,‡] Zsolt Baranyai,[†] Andrés de Blas,[§] Teresa Rodríguez-Blas,[§] István Bányai,[⊥] Carlos Platas-Iglesias,*[,§] and Imre Tóth*[,†]

[†]*Department of Inorganic and Analytical Chemistry, University of Debrecen, P.O. Box 21, Egyetem tér 1, Debrecen H-4010, Hungary,* [§]*Departamento de Química Fundamental, Universidade da Coruña, Campus da Zapateira, Alejandro de la Sota 1, 15008 A Coruña, Spain,* [⊥]*Department of Colloid and Environmental Chemistry, University of Debrecen, P.O. Box 21, Egyetem tér 1, Debrecen H-4010, Hungary, and* [‡]*Research group of Homogeneous Catalysis, MTA-DE, University of Debrecen, Egyetem tér 1, Debrecen H-4032, Hungary*

Received January 29, 2010

The conformational properties of lanthanide(III) complexes with the mono- and biphosphonate analogues of 1,4,7,10-tetraazacyclododecane-1,4,7,10-tetraacetate (DOTA) are investigated by means of density functional theory (DFT) calculations and NMR spectroscopy. Geometry optimizations performed at the B3LYP/6-31G(d) level and using a 46 + $4f^n$ effective core potential for lanthanides provide two energy minima corresponding to the square-antiprismatic (SAP) and twisted square-antiprismatic (TSAP) geometries. Our calculations give relative free energies between the SAP and TSAP isomers in fairly good agreement with the experimental values. The SAP isomer presents the highest binding energy of the ligand to the metal ion, which further increases with respect to that of the TSAP isomer across the lanthanide series as the charge density of the metal ion increases. The stabilization of the TSAP isomer upon substitution of the acetate arms of DOTA by methylenephosphonate ones is attributed to the higher steric demand of the phosphonate groups and the higher strain of the ligand in the SAP isomer. A ^{1}H NMR band-shape analysis performed on the $[Ln(DO2A2P)]^{3-}$ (Ln = La and Lu) complexes provided the activation parameters for enantiomerization of the TSAP form of the complexes. The TSAP isomerization process was also investigated by using DFT calculations on the $[Lu(DOTA)]^-$ and $[Ln(DO2A2P)]^{3-}$ (Ln = La and Lu) systems. Our results confirm that enantiomerization requires both rotation of the pendant arms and inversion of the four five-membered chelate rings formed upon coordination of the macrocyclic unit. According to our calculations, the arm rotation pathway in $[Lu(DOTA)]^-$ is a one-step process involving the simultaneous rotation of the four acetate arms, while in the DO2A2P analogue, the arm-rotation process is a multistep path involving the stepwise rotation of each of the four pendant arms. The calculated activation free energies are in reasonably good agreement with the experimental data. A comparison of the experimental ^{13}C NMR shifts of $[Ln(DO2A2P)]^{3-}$ (Ln=La and Lu) complexes and those calculated by using the GIAO method confirms that the major isomer observed in solution for these complexes corresponds to the TSAP isomer.

Introduction

Complexes of trivalent lanthanide ions with the cyclen derivative 1,4,7,10-tetraazacyclododecane-1,4,7,10-tetraacetate (DOTA; Chart 1) and related ligands are of great interest because of their use in various medical applications, such as cancer radiotherapy[1] or magnetic resonance imaging (MRI).[2] The successful use of these complexes in medical diagnosis and therapy is partially related to their high thermodynamic stability and kinetic inertness.[3]

It is well-known that in Ln^{3+}(DOTA)-like complexes the four ethylenediamine groups adopt gauche conformations,

*To whom correspondence should be addressed. E-mail: imretoth@delfin.unideb.hu (I.T.), cplatas@udc.es (C.P.-I.).

(1) (a) Cutler, C. S.; Smith, C. J.; Ehrhardt, G. J.; Tyler, T. T.; Jurisson, S. S.; Deutsch, E. *Cancer Biother. Radiopharm.* **2000**, *15*, 531–545. (b) Heppeler, A.; Froidevaux, S.; Eberle, A. N.; Maecke, H. R. *Curr. Med. Chem.* **2000**, *7*, 971–994. (c) Heppeler, A.; Froidevaux, S.; Mäcke, H. R.; Jermann, E.; Béhé, M.; Powell, P.; Hennig, M. *Chem.—Eur. J.* **1999**, *5*, 1974–1981.

(2) *The Chemistry of Contrast Agents in Medical Magnetic Resonance Imaging*; Merbach, A. E., Tóth, É., Eds.; Wiley: New York, 2001.

(3) (a) Kumar, K.; Chang, C. A.; Tweedle, M. F. *Inorg. Chem.* **1993**, *32*, 587–593. (b) Kumar, K.; Jin, T.; Wang, X.; Desreux, J. F.; Tweedle, M. F. *Inorg. Chem.* **1994**, *33*, 3823–3829. (c) Brücher, E. *Top. Curr. Chem.* **2002**, *221*, 103–122.

Published on Web 04/06/2010

Chart 1. Ligands Discussed in the Present Work

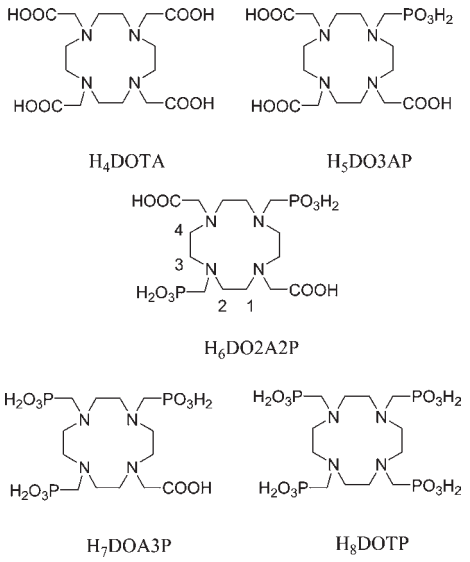

giving rise to two macrocyclic ring conformations: ($\delta\delta\delta\delta$) and ($\lambda\lambda\lambda\lambda$). Furthermore, there are two possible orientations of the four pendant arms (absolute configuration Δ or Λ), resulting in four possible steroisomers, existing as two enantiomeric pairs.[4] These steroisomers differ by the layout of the four acetate arms, adopting either a square-antiprismatic (SAP) or a twisted square-antiprismatic (TSAP) geometry (Figure 1).[5] The two structures display different orientations of the two square planes formed by the four cyclen nitrogen atoms and the four binding oxygen atoms, making an angle of ca. 40° in SAP-type structures, whereas this situation is reversed and reduced to ca. −30° in TSAP-type derivatives.[6] The SAP and TSAP isomers may interconvert in solution by either ring inversion, which leads to a ($\delta\delta\delta\delta$) ↔ ($\lambda\lambda\lambda\lambda$) conformational change, or arm rotation, which results in a $\Delta \leftrightarrow \Lambda$ configurational change. Either process alone interconverts SAP and TSAP geometries, while a combination of the two processes exchanges enantiomeric pairs (Figure 1).[7,8]

Analysis of the NMR spectra of $Ln(DOTA)^-$ complexes has shown that the relative concentration of the two isomers is affected by the nature of the lanthanide ion because the relative stability of the SAP isomer with respect to the TSAP one increases along the lanthanide series.[5] The isomer ratio affects dramatically certain physicochemical properties of the chelate, such as the water exchange rate of the inner-sphere water molecule, an important parameter related to the

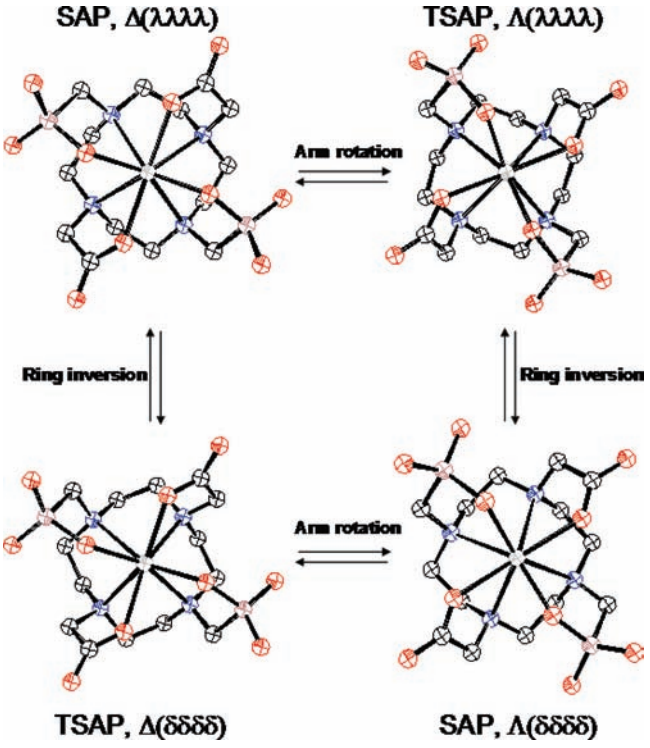

Figure 1. Optimized geometries of the SAP and TSAP isomers of $[Lu(DO2A2P)]^{3-}$. Symbols Δ and Λ refer to the helicity of the pendant arms and δ and λ to that of the macrocycle.[4]

efficiency of MRI contrast agents. The water exchange of the inner-sphere water molecule has been studied on both isomers for several lanthanide(III) complexes with DOTA-like derivatives. It is found that the water exchange on the TSAP isomer is about 2 orders of magnitude faster than that on the SAP one.[9]

Lanthanide complexes with the tetrakis(methylenephosphonate) analogue of DOTA (DOTP; Chart 1) have been investigated in detail.[10] The stability constants of the DOTP complexes are higher than those of the corresponding $[Ln(DOTA)]^-$ complexes,[11] and contrary to the DOTA complexes, DOTP analogues do not contain an inner-sphere water molecule.[12] Ln(DOTP) complexes are known to exist as the TSAP isomer both in the solid state and in solution.[10] More recently, Lukes et al.[13,14] reported the lanthanide

(4) (a) Corey, E. J.; Bailar, J. C., Jr. *J. Am. Chem. Soc.* **1959**, *81*, 2620–2629. (b) Beattie, J. K. *Acc. Chem. Res.* **1971**, *4*, 253–259.
(5) (a) Aime, S.; Botta, M.; Fasano, M.; Marques, M. P. M.; Geraldes, C. F. G. C.; Pubanz, D.; Merbach, A. E. *Inorg. Chem.* **1997**, *36*, 2059–2068. (b) Hoeft, S.; Roth, K. *Chem. Ber.* **1993**, *126*, 869–873. (c) Aime, S.; Botta, M.; Ermondi, G. *Inorg. Chem.* **1992**, *31*, 4291–4299.
(6) Parker, D.; Dickins, R. S.; Puschmann, H.; Crossland, C.; Howard, J. A. K. *Chem. Rev.* **2002**, *102*, 1977–2010.
(7) Jacques, V.; Desreux, J. F. *Inorg. Chem.* **1994**, *33*, 4048–4053.
(8) Aime, S.; Barge, A.; Botta, M.; Fasano, M.; Ayala, J. D.; Bombieri, G. *Inorg. Chim. Acta* **1996**, *246*, 423–429.
(9) (a) Woods, M.; Aime, S.; Botta, M.; Howard, J. A. K.; Moloney, J. M.; Navet, M.; Parker, D.; Port, M.; Rousseaux, O. *J. Am. Chem. Soc.* **2000**, *122*, 9781–9792. (b) Dunand, F. A.; Aime, S.; Merbach, A. E. *J. Am. Chem. Soc.* **2000**, *122*, 1506–1512. (c) Zhang, S.; Kovacs, Z.; Burgess, S.; Aime, S.; Terreno, E.; Sherry, A. D. *Chem.—Eur. J.* **2001**, *7*, 288–296. (d) Woods, M.; Kovacs, Z.; Zhang, S.; Sherry, A. D. *Angew. Chem., Int. Ed.* **2003**, *42*, 5889–5892.
(10) (a) Sherry, A. D.; Malloy, C. R.; Jeffrey, F. M. H.; Cacheris, W. P.; Geraldes, C. F. G. C. *J. Magn. Reson.* **1988**, *76*, 528–533. (b) Rill, C.; Kolar, Z. I.; Kickelbick, G.; Wolterbeek, H. T.; Peters, J. A. *Langmuir* **2009**, *25*, 2294–2301. (c) Yang, T.-H.; Zhou, K.; Bao, S.-S.; Zhu, C.-J.; Zheng, L.-M. *Inorg. Chem. Commun.* **2008**, *11*, 1075–1078. (d) Burai, L.; Kiraly, R.; Lazar, I.; Brucher, E. *Eur. J. Inorg. Chem.* **2001**, 813–820. (e) Corsi, D. M.; van Bekkum, H.; Peters, J. A. *Inorg. Chem.* **2000**, *39*, 4802–4808. (f) Buster, D. C.; Castro, M. M. C. A.; Geraldes, C. F. G. C.; Malloy, C. R.; Sherry, A. D.; Siemers, T. C. *Magn. Reson. Med.* **1990**, *15*, 25–32.
(11) (a) Sherry, A. D.; Ren, J.; Huskens, J.; Bruchner, E.; Toth, E.; Geraldes, C. F. G. C.; Castro, M. M. C. A.; Cacheris, W. P. *Inorg. Chem.* **1996**, *35*, 4604–4612. (b) Delgado, R.; Costa, J.; Guerra, K.; Lima, L. M. P. *Pure Appl. Chem.* **2005**, *77*, 569–579.
(12) (a) Geraldes, C. F. G. C.; Sherry, A. D.; Kiefer, G. E. *J. Magn. Reson.* **1992**, *97*, 290–304. (b) Avecilla, F.; Peters, J. A.; Geraldes, C. F. G. C. *Eur. J. Inorg. Chem.* **2003**, 4179–4186. (c) Botta, M. *Eur. J. Inorg. Chem.* **2000**, 399–407.
(13) Rudovsky, J.; Cigler, P.; Kotek, J.; Hermann, P.; Vojtisek, P.; Lukes, I.; Peters, J. A.; Vander Elst, L.; Muller, R. N. *Chem.—Eur. J.* **2005**, *11*, 2373–2384.
(14) Vojtisek, P.; Cigler, P.; Kotek, J.; Rudovsky, J.; Hermann, P.; Lukes, I. *Inorg. Chem.* **2005**, *44*, 5591–5599.

complexes of the mono(methylenephosphonate) analogue of DOTA (DO3AP; Chart 1). They showed that these complexes contain one inner-sphere water molecule endowed with a very fast water exchange. Ln^{3+}(DO3AP) complexes exist in solution as a mixture of the SAP and TSAP isomers, but the TSAP abundance is significantly higher than that of the corresponding DOTA analogues.[13] The stability of the lanthanide complexes of DO3AP is comparable or somewhat higher than that of the DOTA analogues.[15] Finally, the DO2A2P ligand and its complexes with the trivalent lanthanide ions have also been recently reported by some of us.[16] NMR measurements indicated the absence of an inner-sphere water molecule in these complexes.

The experimental work performed in DOTA-like complexes with the lanthanide ions provides a plethora of information about the solid-state and solution structures of the complexes. However, theoretical investigations performed on these kinds of systems are very much behind the experimental knowledge. Several theoretical investigations of Ln^{III}(DOTA) or DOTA-like complexes based on molecular mechanics,[17] Hartree−Fock (HF),[18] density functional theory (DFT),[19] or molecular dynamics[20] have been reported in the literature. In a seminar paper, Cosentino et al.[21] have reported a conformational characterization of Ln^{III}(DOTA) complexes by using ab initio calculations. They have demonstrated that geometry optimizations performed at the HF level provide calculated structures in good agreement with the experimental ones obtained from X-ray diffraction studies. However, single-point energy calculations at the DFT level (B3LYP model) must be used to obtain relative energies in better agreement with the experimental ones. In subsequent works, we have used a similar computational approach based on HF and/or B3LYP calculations to obtain information at the molecular level on lanthanide complexes with both macrocyclic[22] and acyclic ligands,[23] as well as to predict the ^{13}C NMR spectra of diamagnetic lanthanum(III) and lutetium(III) complexes.

Herein, we report a detailed investigation, based on the B3LYP model, of the conformational properties of several lanthanide complexes with the DO3AP and DO2A2P ligands (Chart 1). We devote special attention to rationalizing the conformational energies of the TSAP and SAP isomers, as well as the mechanism of the TSAP enantiomerization process. Enantiomerization of the TSAP form of $[Ln(DO2A2P)]^{3-}$ complexes (Ln = La or Lu) is also investigated experimentally by using ^{1}H, ^{13}C, and ^{31}P NMR spectroscopy. To understand the effect of the substitution of acetate(s) with methylenephosphonate pendant arm(s) on the relative energies and interconversion mechanism, we also investigate several lanthanide complexes with ligands DOTA, DOA3P, and DOTP and compare our results to experimental data published earlier.[5,10] Finally, the ^{13}C NMR spectrum of $[Ln(DO2A2P)]^{3-}$ (Ln = La or Lu) is investigated by using GIAO calculations, and the results were compared to the corresponding experimental values.

NMR and Computational Methods

NMR Experiments. NMR spectra of $[La(DO2A2P)]^{3-}$ and $[Lu(DO2A2P)]^{3-}$ complexes were measured in 0.03 and 0.08 M samples prepared in D_2O. ^{1}H, ^{13}C, and ^{31}P NMR spectra were collected using either a Bruker DRX 400 (9.4 T) or a Bruker DMX 500 (11.75 T) NMR spectrometer. Variable-temperature ^{1}H and ^{13}C NMR measurements were carried out using the Bruker DRX 400 NMR spectrometer equipped with a Bruker VT-1000 thermocontroller and a BB inverse *z*-gradient probe (5 mm). The chemical shifts were reported in ppm referring to tetramethylsilane (TMS) for ^{1}H and ^{13}C NMR and to 85% (m/m) H_3PO_4 for ^{31}P NMR as external standards. The $^{1}H-^{1}H$ correlation spectroscopy (COSY) and exchange spectroscopy (EXSY) spectra were collected by using gradient pulses in the *z* direction with the standard Bruker pulse program [in the case of EXSY spectra, the mixing time (τ_M) was 500 ms]. The $^{1}H-^{13}C$ correlation spectra were recorded on a Bruker DRX 400 NMR spectrometer by using gradient pulse in the *z* direction with the usual Bruker heteronuclear single quantum coherence (HSQC) pulse sequence.

Band-shape analyses were performed by using the NMR-Sim program included in the Bruker WIN-NMR software package. The signals of $4H_a$ and $4H_e$ ring protons and 5H and 6H acetate methylene protons were simulated. Values of the chemical shift, the spin−spin

(15) Taborsky, P.; Lubal, P.; Havel, J.; Kotek, J.; Hermann, P.; Lukes, I. *Collect. Czech. Chem. Commun.* **2005**, *70*, 1909–1942.
(16) Kalman, F. K.; Baranyai, Z.; Toth, I.; Banyai, I.; Kiraly, R.; Brucher, E.; Aime, S.; Sun, X.; Sherry, A. D.; Kovacs, Z. *Inorg. Chem.* **2008**, *47*, 3851–3862.
(17) (a) Henriques, E. S.; Geraldes, C. F. G. C.; Ramos, M. J. *Mol. Phys.* **2003**, *101*, 2319–2333. (b) Ranganathan, R. S.; Raju, N.; Fan, H.; Zhang, X.; Tweedle, M. F.; Desreux, J. F.; Jacques, V. *Inorg. Chem.* **2002**, *41*, 6856–6866. (c) Chang, C. A.; Liu, C. Y.-L.; Chen, C.-Y.; Chou, X.-M. *Inorg. Chem.* **2001**, *40*, 3448–3455. (d) Fossheim, R.; Dugstad, H.; Dahl, S. G. *Eur. J. Med. Chem.* **1995**, *30*, 539–546. (e) Fossheim, R.; Dahl, S. G. *Acta Chem. Scand.* **1990**, *44*, 698–706.
(18) (a) Henriques, E. S.; Bastos, M.; Geraldes, C. F. G. C.; Ramos, M. J. *Int. J. Quantum Chem.* **1999**, *73*, 237–248. (b) Cosentino, U.; Moro, G.; Pitea, D.; Villa, A.; Fantucci, P. C.; Maiocchi, A.; Uggeri, F. *J. Phys. Chem. A* **1998**, *102*, 4606–4614.
(19) (a) Hess, B. A., Jr.; Kedziorski, A.; Smentek, L.; Bornhop, D. J. *J. Phys. Chem. A* **2008**, *112*, 2397–2407. (b) Yazyev, O. V.; Helm, L.; Malkin, V. G.; Malkina, O. L. *J. Phys. Chem. A* **2005**, *109*, 10997–11005. (c) Smentek, L.; Hess, B. A., Jr.; Cross, J. P.; Manning, H. C.; Bornhop, D. J. *J. Chem. Phys.* **2005**, *123*, 244302.
(20) (a) Yazyev, O. V.; Helm, L. *Eur. J. Inorg. Chem.* **2008**, 201–211. (b) Yerly, F.; Borel, A.; Helm, L.; Merbach, A. E. *Chem.—Eur. J.* **2003**, *9*, 5468–5480. (c) Borel, A.; Helm, L.; Merbach, A. E. *Chem.—Eur. J.* **2001**, *7*, 600–610.
(21) Cosentino, U.; Villa, A.; Pitea, D.; Moro, G.; Barone, V.; Maiocchi, A. *J. Am. Chem. Soc.* **2002**, *124*, 4901–4909.
(22) (a) Roca-Sabio, A.; Mato-Iglesias, M.; Esteban-Gomez, D.; Toth, E.; de Blas, A.; Platas-Iglesias, C.; Rodríguez-Blas, T. *J. Am. Chem. Soc.* **2009**, *131*, 3331–3341. (b) Mato-Iglesias, M.; Roca-Sabio, A.; Palinkas, Z.; Esteban-Gomez, D.; Platas-Iglesias, C.; Toth, E.; de Blas, A.; Rodriguez-Blas, T. *Inorg. Chem.* **2008**, *47*, 7840–7851. (c) Fernandez-Fernandez, M. del C.; Bastida, R.; Macias, A.; Perez-Lourido, P.; Platas-Iglesias, C.; Valencia, L. *Inorg. Chem.* **2006**, *45*, 4484–4496. (d) Gonzalez-Lorenzo, M.; Platas-Iglesias, C.; Avecilla, F.; Faulkner, S.; Pope, S. J. A.; de Blas, A.; Rodriguez-Blas, T. *Inorg. Chem.* **2005**, *44*, 4254–4262. (e) Nuñez, C.; Bastida, R.; Macias, A.; Mato-Iglesias, M.; Platas-Iglesias, C.; Valencia, L. *Dalton Trans.* **2008**, 3841–3850. (f) Nuñez, C.; Mato-Iglesias, M.; Bastida, R.; Macias, A.; Perez-Lourido, P.; Platas-Iglesias, C.; Valencia, L. *Eur. J. Inorg. Chem.* **2009**, 1086–1095. (g) Gonzalez-Lorenzo, M.; Platas-Iglesias, C.; Mato-Iglesias, M.; Esteban-Gomez, D.; de Blas, A.; Rodriguez-Blas, T. *Polyhedron* **2008**, *27*, 1415–1422.
(23) (a) Platas-Iglesias, C.; Mato-Iglesias, M.; Djanashvili, K.; Muller, R. N.; Vander Elst, L.; Peters, J. A.; de Blas, A.; Rodriguez-Blas, T. *Chem.—Eur. J.* **2004**, *10*, 3579–3590. (b) Mato-Iglesias, M.; Rodríguez-Blas, T.; Platas-Iglesias, C.; Starck, M.; Kadjane, P.; Ziessel, R.; Charbonniere, L. *Inorg. Chem.* **2009**, *48*, 1507–1518. (c) Charbonniere, L.; Mameri, S.; Kadjane, P.; Platas-Iglesias, C.; Ziessel, R. *Inorg. Chem.* **2008**, *47*, 3748–3762. (d) Mato-Iglesias, M.; Platas-Iglesias, C.; Djanashvili, K.; Peters, J. A.; Toth, E.; Balogh, E.; Muller, R. N.; Vander Elst, L.; de Blas, A.; Rodriguez-Blas, T. *Chem. Commun.* **2005**, 4729–4731. (e) Mato-Iglesias, M.; Balogh, E.; Platas-Iglesias, C.; Toth, E.; de Blas, A.; Rodriguez-Blas, T. *Dalton Trans.* **2006**, 5404–5415.

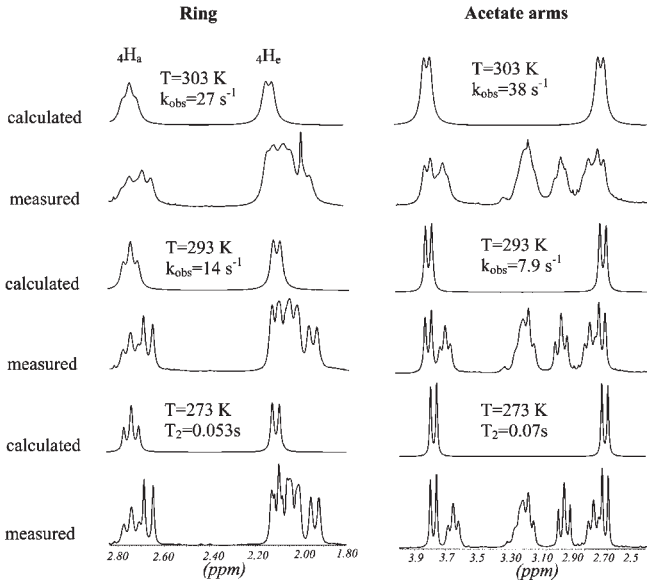

Figure 2. Experimental and calculated ^{1}H NMR spectra of $[La(DO2A2P)]^{3-}$ (400 MHz, pD = 9.8, [LaL] = 0.03 M) used for band-shape analysis in the temperature range 273−303 K.

coupling constants (see Table S1 in the Supporting Information for the lanthanum complex and ref 16 for the lutetium complex), and the transversal relaxation time without chemical exchange (measured at 273 K; see Figure 2) were fixed input parameters, while the value of $^*T_2$ was varied. The k_{obs} values were calculated from the $^*T_2$ values by using to the following equations:

$$\frac{1}{^*T_2} = \frac{1}{T_2} + \frac{1}{\tau} = \frac{T_2 + \tau}{T_2 \tau} \quad (1)$$

$$k_{obs} = \frac{1}{\tau} \quad (2)$$

where τ, k_{obs}, $^*T_2$, and T_2 are the averaged lifetime, the rate of the exchange processes, and the transversal relaxation times with and without exchange processes, respectively. These particular signals were selected for simulations because these were found in less crowded regions of the ^{1}H NMR spectrum. A comparison of the measured and calculated spectra at different temperature values was done by visual observation, focusing on the given spin system; i.e., the overlapping signals not involved in the simulation were not directly considered.

Computational Methods. All calculations were performed employing hybrid DFT with the B3LYP exchange-correlation functional,[24,25] and the *Gaussian 03* package (revision C.01).[26] Full geometry optimizations of the $[Ln(DOTA)(H_2O)]^-$, $[Ln(DO3AP)(H_2O)]^{2-}$, $[Ln(HDO3AP)(H_2O)]^-$, $[Ln(DO2A2P)]^{3-}$, $[Ln(DOA3P)]^{4-}$, and $[Ln(DOTP)]^{5-}$ systems were performed in vacuo by using the 6-31G(d) basis set for carbon, hydrogen, nitrogen, oxygen, and phosphorus atoms. Different computational studies on lanthanide(III) complexes have shown that the 4f orbitals do not participate in bonding because of their contraction into the core.[27] As a consequence, no effect of the spin−orbit coupling on the equilibrium geometries of lanthanide(III) complexes was found.[28] Thus, spin−orbit effects were not taken into account in the present work. Relativistic effects were considered through the use of relativistic effective core potentials (RECPs). Therefore, for the lanthanides, the quasi-relativistic effective core potential (ECP) of Dolg et al. and the related [5s4p3d]-GTO valence basis set were applied.[29] This ECP treats $[Kr]4d^{10}4f^n$ as fixed cores, while only the $5s^25p^66s^25d^16p^0$ shell is taken into account explicitly. It had been demonstrated that this ECP provided reliable results for several lanthanide complexes, including the Ln^{3+} aquo ions[30,31] and complexes with both macrocyclic[22,32] and acyclic[23,33] ligands. Compared to all-electron basis sets, ECPs account to some extent for relativistic effects, which are believed to become important for the elements from the fourth row of the periodic table. No symmetry constraints have been imposed during the optimizations. The default values for the integration grid ("fine") and the self-consistent-field energy convergence criteria (10^{-6}) were used. The stationary points found on the potential energy surfaces as a result of the geometry optimizations had been tested to represent energy minima rather than saddle points via frequency analysis.

The geometries of the $[Nd(HDO3AP)(H_2O)]^-$ and $[Er(HDO3AP)]^-$ systems were fully optimized in an aqueous solution by using a polarizable continuum model (PCM). In particular, we used the C-PCM variant,[34] which, employing conductor rather than dielectric boundary conditions, allows a more robust implementation. The solute cavity was built as an envelope of spheres centered on atoms or atomic groups with appropriate radii. Each sphere was subdivided into 60 initial tesserae in pentakisdodecahedral patterns. Calculations were

(24) Becke, A. D. *J. Chem. Phys.* **1993**, *98*, 5648–5652.
(25) Lee, C.; Yang, W.; Parr, R. G. *Phys. Rev. B* **1988**, *37*, 785–789.
(26) Frisch, M. J.; Trucks, G. W.; Schlegel, H. B.; Scuseria, G. E.; Robb, M. A.; Cheeseman, J. R.; Montgomery, J. A., Jr.; Vreven, T.; Kudin, K. N.; Burant, J. C.; Millam, J. M.; Iyengar, S. S.; Tomasi, J.; Barone, V.; Mennucci, B.; Cossi, M.; Scalmani, G.; Rega, N.; Petersson, G. A.; Nakatsuji, H.; Hada, M.; Ehara, M.; Toyota, K.; Fukuda, R.; Hasegawa, J.; Ishida, M.; Nakajima, T.; Honda, Y.; Kitao, O.; Nakai, H.; Klene, M.; Li, X.; Knox, J. E.; Hratchian, H. P.; Cross, J. B.; Bakken, V.; Adamo, C.; Jaramillo, J.; Gomperts, R.; Stratmann, R. E.; Yazyev, O.; Austin, A. J.; Cammi, R.; Pomelli, C.; Ochterski, J. W.; Ayala, P. Y.; Morokuma, K.; Voth, G. A.; Salvador, P.; Dannenberg, J. J.; Zakrzewski, V. G.; Dapprich, S.; Daniels, A. D.; Strain, M. C.; Farkas, O.; Malick, D. K.; Rabuck, A. D.; Raghavachari, K.; Foresman, J. B.; Ortiz, J. V.; Cui, Q.; Baboul, A. G.; Clifford, S.; Cioslowski, J.; Stefanov, B. B.; Liu, G.; Liashenko, A.; Piskorz, P.; Komaromi, I.; Martin, R. L.; Fox, D. J.; Keith, T.; Al-Laham, M. A.; Peng, C. Y.; Nanayakkara, A.; Challacombe, M.; Gill, P. M. W.; Johnson, B.; Chen, W.; Wong, M. W.; Gonzalez, C.; Pople, J. A. *Gaussian 03*, revision C.01; Gaussian, Inc.: Wallingford, CT, 2004.
(27) (a) Maron, L.; Eisenstein, O. *J. Phys. Chem. A* **2000**, *104*, 7140–7143. (b) Boehme, C.; Coupez, B.; Wipff, G. *J. Phys. Chem. A* **2002**, *106*, 6487–6498. (c) Ingram, K. I. M.; Tassell, M. J.; Gaunt, A. J.; Kaltsoyannis, N. *Inorg. Chem.* **2008**, *47*, 7824–7833.
(28) Vetere, V.; Maldivi, P.; Adamo, C. *J. Comput. Chem.* **2003**, *24*, 850–858.
(29) Dolg, M.; Stoll, H.; Savin, A.; Preuss, H. *Theor. Chim. Acta* **1989**, *75*, 173–194.
(30) Djanashvili, K.; Platas-Iglesias, C.; Peters, J. A. *Dalton Trans.* **2008**, 602–607.
(31) (a) Dinescu, A.; Clark, A. E. *J. Phys. Chem. A* **2008**, *112*, 11198–11206. (b) Clark, A. E. *J. Chem. Theory Comput.* **2008**, *4*, 708–718.
(32) (a) Perez-Mayoral, E.; Soriano, E.; Cerdan, S.; Ballesteros, P. *Molecules* **2006**, *11*, 345–356. (b) Guillaumont, D.; Bazin, H.; Benech, J.-M.; Boyer, M.; Mathis, G. *ChemPhysChem* **2007**, *8*, 480–488.
(33) (a) Quali, N.; Bocquet, B.; Rigault, S.; Morgantini, P.-Y.; Weber, J.; Piguet, C. *Inorg. Chem.* **2002**, *41*, 1436–1445. (b) De Silva, C. R.; Li, J.; Zheng, Z.; Corrales, L. R. *J. Phys. Chem. A* **2008**, *112*, 4527–4530.
(34) Barone, V.; Cossi, M. *J. Phys. Chem. A* **1998**, *102*, 1995–2001.

performed using an average area of 0.2 Å^2 for all the finite elements (tesserae) used to build the solute cavities. For lanthanides, the previously parametrized radius was used.[35] Owing to the slow convergence of the optimizations,[36] they were stopped when the convergence parameters were about twice the default values.[37] For this reason, frequency analysis was not performed to characterize the stationary points; thus, the final geometries correspond to stable conformations for the chosen minimization algorithm rather than to true minima.

Binding energies (BE) of the macrocyclic ligands in the corresponding complexes were calculated as the energy of the complex less than that of the metal ion and that of the ligand, with the ligand at the geometry found within the complex. Therefore, the BEs were static because they did not include energy contributions due to changes in the ligand geometry. Basis set superposition errors (BSSEs) were calculated using the standard counterpoise method.[38] BSSE is an undesirable consequence of using finite basis sets that leads to an overestimation of the BE. Relative strain energies (SEs) were calculated as the relative energies of the ligands in their geometry found within the SAP and TSAP complexes.

The relative free energies of the SAP and TSAP conformations were calculated in vacuo at the B3LYP/6-31G(d) level, including non-potential-energy contributions (zero-point energies and thermal terms) obtained through frequency analysis. The interconversion between the SAP and TSAP conformations of the [Ln(DO2A2P)]$^{3-}$ and [Lu(DOTA)]$^-$ complexes was investigated in vacuo by means of the synchronous transit-guided quasi-Newton method.[39] The nature of the saddle points and intermediates was characterized by frequency analysis. The relative energy barriers calculated in vacuo include non-potential-energy contributions (that is, zero-point energies and thermal terms) obtained by frequency analysis.

The NMR shielding tensors (GIAO[40] method) of the [Lu(DO2A2P)]$^{3-}$ system were calculated in vacuo at the B3LYP functional level. Previous investigations had shown that the (46 + 4f^n)-core-electron ECP of Dolg et al. provided inconsistent ^{13}C NMR chemical shifts.[21] Thus, in our calculation, the 46-core-electron ECP of Stevens et al.[41,42] was used, leaving the 4f^{14} electrons in the valence, in combination with the 6-311G** basis set for the ligand atoms. For chemical shift calculation purposes, NMR shielding tensors of TMS were calculated at the same computational level.

(35) Cosentino, U.; Villa, A.; Pitea, D.; Moro, G.; Barone, V. *J. Phys. Chem. B* **2000**, *104*, 8001–8007.
(36) (a) Tsushima, S.; Yang, T.; Mochizuki, Y.; Okamoto, Y. *Chem. Phys. Lett*. **2003**, *375*, 204–212. (b) Li, H.; Jensen, J. H. *J. Comput. Chem*. **2004**, *25*, 1449–1462.
(37) Cosentino, U.; Moro, G.; Pitea, D.; Barone, V.; Villa, A.; Muller, R. N.; Botteman, F. *Theor. Chem. Acc*. **2004**, *111*, 204–209.
(38) Bernardi, F.; Boys, S. F. *Mol. Phys*. **1970**, *19*, 553–566.
(39) (a) Peng, C.; Ayala, P. Y.; Schlegel, H. B.; Frisch, M. J. *J. Comput. Chem*. **1996**, *17*, 49–56. (b) Peng, C.; Schlegel, H. B. *Isr. J. Chem*. **1994**, *33*, 449–454.
(40) Ditchfield, R. *Mol. Phys*. **1974**, *27*, 789–807.
(41) Stevens, W. J.; Krauss, M.; Basch, H.; Jaisen, P. G. *Can. J. Chem*. **1992**, *70*, 612–630.
(42) Cundari, T. R.; Stevens, W. *J. Chem. Phys*. **1993**, *98*, 5555–5565.

Table 1. Rate Constants and Activation Parameters for the Ring-Inversion and Arm-Rotation Processes of [Ln(DO2A2P)]$^{3-}$ (Ln = La and Lu) Complexes Obtained from the Line-Shape Analysis of the ^{1}H NMR Spectra

	La		Lu	
	arm rotation	ring inversion	arm rotation	ring inversion[a]
$\Delta H^{\ddagger}$/kcal·mol^{-1}	26.1 ± 0.2	9.3 ± 0.7	30.4 ± 2.5	14.4 ± 0.9
$\Delta S^{\ddagger}$/cal·mol^{-1}·K^{-1}	34.7 ± 1.0	−21.4 ± 2.4	49.2 ± 8.1	−3.4 ± 2.9
$\Delta G^{\ddagger}_{298}$/kcal·mol^{-1}	15.5 ± 0.2	15.7 ± 3.0	15.7 ± 2.4	15.4 ± 0.9
k_{obs}^{298}/s^{-1}	18.7 ± 1.0	19.7 ± 1.0	20.1 ± 1.0	31.3 ± 1.0

[a] Reference 16.

Results and Discussion

NMR Studies. The protonation and complexation properties of the ligand DO2A2P, the kinetics of formation and dissociation of some [Ln(DO2A2P)]$^{3-}$ complexes, and the solution structures of [Eu(DO2A2P)]$^{3-}$ and [Lu(DO2A2P)]$^{3-}$ complexes have been studied in detail, and the results were published in our previous paper.[16] The 1D (^{1}H, ^{13}C, and ^{31}P NMR) spectra, the 2D spectra (COSY, EXSY and HSQC), as well as the variable-temperature ^{1}H and ^{13}C NMR spectra of the [Eu(DO2A2P)]$^{3-}$ and the [Lu(DO2A2P)]$^{3-}$ complexes have revealed the presence of the TSAP isomer as the major form in solution. The rate constant and the activation parameters for the inversion of the macrocylic ring in [Lu(DO2A2P)]$^{3-}$ have been determined by carrying out a line-shape analysis on the signals attributed to the 4H protons (see Chart 1 for labeling). A closer inspection of the variable-temperature ^{1}H NMR spectra of [Lu(DO2A2P)]$^{3-}$ allows the determination of the activation parameters and rate constant for the arm-rotation process. Indeed, a band-shape analysis performed on protons C*H*$_2$COO$^-$ provided the activation parameters given in Table 1. The analysis performed on the C*H*$_2$PO$_3^{2-}$ protons provides essentially the same parameters, within the error margins of the technique. Furthermore, we have performed NMR studies on the [La(DO2A2P)]$^{3-}$ complex to investigate the effect of the size of the Ln^{3+} ion on the isomerization processes of [Ln(DO2A2P)]$^{3-}$ complexes. The ^{1}H and ^{13}C NMR spectra of the [La(DO2A2P)]$^{3-}$ complex (Figures S1 and S2 in the Supporting Information) are very similar to those of [Lu(DO2A2P)]$^{3-}$, which indicates the predominant presence of the TSAP isomer in solution. The ^{1}H and ^{13}C NMR spectra of the [La(DO2A2P)]$^{3-}$ complex are assigned using various 2D NMR techniques [COSY, EXSY, and heteronuclear single quantum coherence (HSQC); Figures S3−S6 in the Supporting Information] at different temperatures. The method followed for the assignment of the spectra is identical with that reported for the Lu^{3+} analogue.[16] The assignments of the proton signals and the relevant coupling constants are given in Table S1 in the Supporting Information. A band-shape analysis of signals 4H provides activation parameters for the ring-inversion process in the [La(DO2A2P)]$^{3-}$ complex. As for the Lu^{3+} analogue, the band-shape analysis of the signals of C*H*$_2$COO$^-$ protons provides the activation parameters for the rotation of the pendant arms (Figure 2).

A striking feature of our band-shape analysis is that we obtain different activation parameters from the Eyring plots for the rotation of the pendant arms and the ring

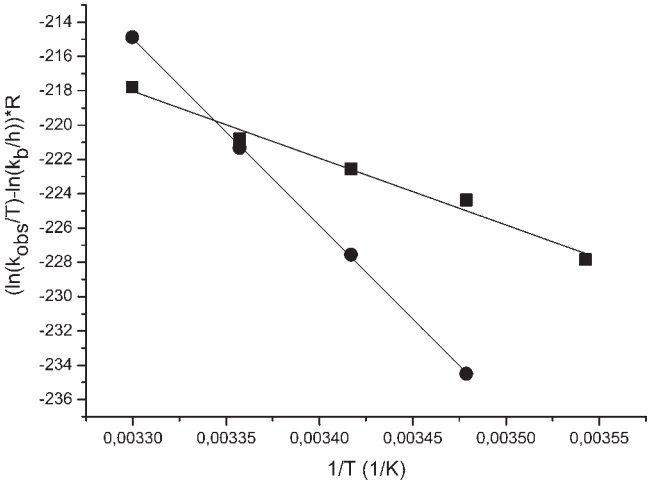

Figure 3. Eyring plots for determining the activation parameters of the ring-inversion (squares) and arm-rotation (circles) processes in $[La(DO2A2P)]^{3-}$.

inversion (Figure 3). Our band-shape analysis provides very similar activation free energies ($\Delta G^{\ddagger}_{298}$) but very different $\Delta H^{\ddagger}$ and $\Delta S^{\ddagger}$ values for the two processes. The fact that we observe two different exchange processes with different activation parameters is clearly confirmed by the different interconversion rates obtained at the same temperature from the band-shape analysis of protons 4H and CH_2COO^- (Figure 2), as well as from the very different slopes and intercepts obtained from the Eyring plots (Figure 3).

For both the lanthanum(III) and lutetium(III) complexes, there is a dominant diastereoisomer in solution consisting of the enantiomeric pair $\Delta(\delta\delta\delta\delta)$ and $\Lambda(\lambda\lambda\lambda\lambda)$. The concentration of the other enantiomeric pair $[\Delta(\lambda\lambda\lambda\lambda)/\Lambda(\delta\delta\delta\delta)]$ is so low that its presence in solution could not be detected by NMR. The interconversion of the enantiomeric pair observed in solution is expected to occur through two consecutive equilibria: $\Delta(\delta\delta\delta\delta) \leftrightarrows \Delta(\lambda\lambda\lambda\lambda) \leftrightarrows \Lambda(\lambda\lambda\lambda\lambda)$ [or $\Lambda(\lambda\lambda\lambda\lambda) \leftrightarrows \Lambda(\delta\delta\delta\delta) \leftrightarrows \Delta(\delta\delta\delta\delta)$]. The exchange process responsible for the line broadening of protons 4H at low temperature is attributed to the first step of the enantiomerization pathway. At low temperature, the rate of the first step is faster than that of the second one, and two consecutive ring-inversion processes follow each other many times before arm rotation happens. This means that a ring inversion occurs, leading to a SAP intermediate, but the enantiomerization process is not completed, so that a second ring-inversion process brings the complex to its original conformation. The exchange process that leads to the broadening of the CH_2COO^- and $CH_2PO_3^{2-}$ protons is attributed to a $\Delta(\delta\delta\delta\delta) \leftrightarrows \Lambda(\lambda\lambda\lambda\lambda)$ interconversion. This requires the inversion of the cyclen ring either before $[\Lambda(\lambda\lambda\lambda\lambda) \leftrightarrows \Lambda(\delta\delta\delta\delta) \leftrightarrows \Delta(\delta\delta\delta\delta)]$ or after $[\Lambda(\lambda\lambda\lambda\lambda) \leftrightarrows \Delta(\lambda\lambda\lambda\lambda) \leftrightarrows \Delta(\delta\delta\delta\delta)]$ the rate-determining rotation of the pendant arms at lower temperature (Figure 1). The big differences in the $\Delta H^{\ddagger}$ and $\Delta S^{\ddagger}$ values obtained for the ring-inversion and arm-rotation processes cause at lower temperatures the ring inversion to be the fastest process, while at 298 K, they are characterized by very similar $\Delta G^{\ddagger}_{298}$ and k_{obs}^{298} values. Thus, the enthalpy-controlled arm-rotation process is the rate-determining step for the enantiomerization process at low temperatures, but because of activation entropy control, the ring-inversion process becomes the rate-determining step at high temperatures. A similar situation in which different molecular motions predominate, depending on the temperature, has been observed for the $[K(DOTA)]^{3-}$ complex.[43]

We obtain very similar $\Delta G^{\ddagger}_{298}$ and k_{obs}^{298} values for the lanthanum(III) and lutetium(III) complexes, which indicates that the arm-rotation and ring-inversion processes are relatively insensitive to the size of the encapsulated ion. A similar conclusion was obtained from the investigation of the ring-inversion processes in the Ln^{3+}-(DOTA) analogues.[44] The arm-rotation process presents higher $\Delta H^{\ddagger}$ values than the inversion of the macrocyclic ring. Most likely, this is because the arm-rotation process requires a weakening of the bonds formed between the lanthanide and the hard, negatively charged oxygen donor atoms, while the inversion of the macrocycle affects the bonds formed between the lanthanide and the neutral nitrogen donor atoms of the macrocycle. The rotation of the pendant arms is characterized by positive activation entropy values, which is probably related to a reorganization of the second-sphere hydration shell around the negatively charged oxygen donor atoms in the transition state. On the contrary, the ring-inversion process is associated with negative $\Delta S^{\ddagger}$ values. Although we do not have a straightforward explanation for the negative $\Delta S^{\ddagger}$ values obtained for the ring-inversion process, a similar situation was observed for the $[K(DOTA)]^{3-}$ and $[Bi(DOTA)]^-$ complexes.[43,45]

A comparison of the activation free energy obtained for the ring-inversion process in $[Ln(DO2A2P)]^{3-}$ complexes (15.7 and 15.4 kcal·mol^{-1} for lanthanum and lutetium, respectively) with that obtained for $[La(DOTP)]^{5-}$ (24.1 kcal·mol^{-1})[46] indicates that the replacement of two opposite methylenephosphonate pendants of $[Ln(DOTP)]^{5-}$ with two acetate arms decreases the rigidity of the macrocyclic ring. However, the activation free energies obtained for the ring-inversion and arm-rotation processes of DO2A2P complexes are very similar to those obtained for the DOTA analogues.[7,8]

DFT-Optimized Geometries. Lukes et al.[13,14] reported several X-ray structures of lanthanide complexes with the HDO3AP ligand, in which the phosphonate group was protonated. They found that the neodymium and terbium complexes contained an inner-sphere water molecule, while in the dysprosium, erbium, and lutetium analogues, the metal ion was eight-coordinated with no inner-sphere water molecule. Thus, we have performed full geometry optimizations of the $[Nd(HDO3AP)(H_2O)]^-$ and $[Er(HDO3AP)]^-$ systems at the B3LYP level. Our calculations provide the SAP and TSAP isomers as minimum-energy conformations. The main calculated geometrical parameters are compared to the experimental data obtained for the TSAP isomer in Table 2. The average Ln−O distances obtained from DFT calculations are in

(43) Csajbok, E.; Banyai, I.; Brucher, E. *Dalton Trans.* **2004**, 2152–2156.
(44) Desreux, J. F. *Inorg. Chem.* **1980**, *19*, 1319–1324.
(45) Csajbok, E.; Baranyai, Z.; Banyai, I.; Brucher, E.; Kiraly, R.; Muller-Fahrnow, A.; Platzek, J.; Raduchel, B.; Schafer, M. *Inorg. Chem.* **2003**, *42*, 2342–2349.
(46) Geraldes, C. F. G. C.; Sherry, A. D.; Kiefer, G. E. *J. Magn. Reson.* **1992**, *97*, 290–304.

Table 2. Geometrical Parameters of Calculated Structures for the Two Isomers of $[Ln(HDO3AP)(H_2O)_q]^-$ Complexes (Ln = Nd, q = 1; Ln = Er, q = 0)[a]

	Nd			Er		
	SAP calcd	TSAP calcd	TSAP exptl	SAP calcd	TSAP calcd	TSAP exptl
Ln−N	2.838	2.859	2.721	2.720	2.736	2.554
Ln−O	2.432	2.430	2.426	2.275	2.296	2.293
$Ln-O_W$	2.641	2.627	2.591			
ω[b]	38.2	−26.2	−26.0	39.5	−27.2	−24.9
$Ln-P_O$[c]	0.641	0.676	0.792	0.768	0.819	1.054
$Ln-P_N$[d]	1.840	1.890	1.746	1.681	1.733	1.472
P_O-P_N[e]	2.480	2.568	2.536	2.448	2.552	2.525

[a] Distances (Å). The average values of the bond distances to the oxygen atoms of the P_O (Ln−O) and P_N (Ln−N) planes are reported; O_W, oxygen atom of the inner-sphere water molecule. [b] Mean twist angle (deg) of the upper and lower planes. [c] Distance between the lanthanide and the least-squares plane defined by the coordinated oxygen atoms, P_O. [d] Distance between the lanthanide and the least-squares plane defined by the nitrogen atoms, P_N. [e] Distance between the centroids of the P_O and P_N planes.

excellent agreement with the experimental values. The coordination polyhedron around the lanthanide ion may be considered to be comprised of two virtually parallel pseudoplanes: the four amine nitrogen atoms define the lower plane (P_N), while the four oxygen atoms coordinated to the metal ion define the upper plane (P_O). The mean twist angles of these parallel planes obtained for the TSAP isomer are in very good agreement with the experimental values. The main discrepancy between the experimental and calculated geometries arises from the Ln−N distances. Indeed, the optimized geometries present substantially longer Ln−N bond distances than the solid-state structures, which is also reflected in the $Ln-P_N$ and $Ln-P_O$ values. This can be partially ascribed to the fact that the large-core ECPs usually provide bond distances ca. 0.02−0.07 Å longer than the experimental ones.[47] To test the effect of the solvent in the geometries of these complexes, we have performed geometry optimizations in an aqueous solution by using a PCM. However, it is well-known that geometry optimizations in solution based on the PCM model suffer from convergence problems such as slow convergence, no convergence, or convergence to higher energetic conformations.[36,37] In our case, full convergence of the optimizations was not reached, and thus the calculated geometries should be considered as stable conformations for the chosen minimization algorithm rather than energy minima. However, our results show that the inclusion of solvent effects results in a relatively important shortening of the Ln−N bond distances (ca. 0.07−0.08 Å), while the Ln−O bonds are only slightly increased (ca. 0.03 Å). Thus, we hold the view that our calculations performed in the gas phase overestimate the Ln−N bond distances with respect to the solution phase. A dramatic shortening of the metal−N bond distances upon solvent inclusion has been recently observed for indium(III) and gallium(III) complexes with functionalized triazamacrocycles.[48] One of the goals of this work is to study the enantiomerization of the TSAP isomer, which requires characterization of energy minima and transition states by using frequency analysis. Thus, in the following, we will focus on the geometries of the different complexes optimized in the gas phase.

Table 3. Geometrical Parameters of Calculated Structures for the Two Isomers of $[Ln(DO2A2P)]^{3-}$ Complexes (Ln = La, Eu, or Lu)[a]

	La		Eu		Lu	
	SAP	TSAP	SAP	TSAP	SAP	TSAP
$Ln-N_{CCO}$	2.946	2.943	2.874	2.871	2.831	2.832
$Ln-N_{CPO}$	2.906	3.022	2.843	2.957	2.806	2.935
$Ln-O_{CO}$	2.547	2.553	2.437	2.440	2.323	2.325
$Ln-O_{PO}$	2.385	2.369	2.273	2.261	2.165	2.154
ω[b]	35.4	−20.3	36.6	−22.5	38.3	−24.2
$Ln-P_O$[c]	0.679	0.750	0.712	0.767	0.716	0.750
$Ln-P_N$[d]	1.955	2.042	1.870	1.980	1.832	1.950

[a] Distances (Å). N_{CCO}, amine nitrogen atom attached to the acetate groups; N_{CPO}, amine nitrogen atom attached to the methylenephosphonate group; O_{CO}, oxygen atom of a carboxylate group; O_{PO}, oxygen atom of a phosphonate group. [b] Mean twist angle (deg) of the upper and lower planes. [c] Distance between the lanthanide and the least-squares plane defined by the coordinated oxygen atoms, P_O. [d] Distance between the lanthanide and the least-squares plane defined by the nitrogen atoms, P_N.

^{17}O NMR and relaxivity studies performed on the $[Gd(DO2A2P)]^{3-}$ complex have demonstrated the absence of inner-sphere water molecules in the complex. Thus, we performed full geometry optimizations of the $[Ln(DO2A2P)]^{3-}$ systems (Ln = La, Eu, or Lu) by using the B3LYP model. As expected, geometry optimizations provide two minimum-energy conformations corresponding to the TSAP and SAP isomers. Calculated bond distances of the metal coordination environments are listed in Table 3. The optimized geometries present a nearly undistorted C_2 symmetry, with the symmetry axis being perpendicular to the mean plane described by the four amine nitrogen atoms and containing the lanthanide ion (Figure 1). The distances between the metal ions and the donor atoms of the ligand decrease along the lanthanide series, as is usually observed for lanthanide(III) complexes as a consequence of the lanthanide contraction.[49]

The distances between the metal ion and the oxygen atoms of the pendant arms are very similar for both the SAP and TSAP isomers. However, the distance to the amine nitrogen atoms attached to the methylenephosphonate groups is clearly longer in the TSAP isomer than in the SAP one. Thus, the interaction between the ligand and the donor atoms of the macrocycle appears to be weaker in the TSAP isomer than in the SAP one. The presence of two different pendant arms results in large deviations from planarity of the oxygen atoms describing the P_O plane (0.13−0.23 Å). The oxygen atoms of the phosphonate groups and those of the acetate groups are placed respectively above and below the mean plane. The mean twist angles ω[50] between the two parallel squares amount to ca. 35−38° and −20 to −24° in the SAP and TSAP isomers, respectively. These values are very similar to those observed in the solid state for the respective isomers of DOTA complexes.[21]

(47) (a) Heiberg, H.; Gropen, O.; Laerdahl, J. K.; Swang, O.; Wahlgren, U. *Theor. Chem. Acc.* **2003**, *110*, 118–125. (b) Buzko, V.; Sukhno, I.; Buzko, M. *THEOCHEM* **2009**, *894*, 75–79.

(48) Notni, J.; Pohle, K.; Peters, J. A.; Gorls, H.; Platas-Iglesias, C. *Inorg. Chem.* **2009**, *48*, 3257–3267.

(49) Seitz, M.; Oliver, A. G.; Raymond, K. N. *J. Am. Chem. Soc.* **2007**, *129*, 11153–11160.

(50) Piguet, C.; Bünzli, J.-C. G.; Bernardinelli, G.; Bochet, C. G.; Froidevaux, P. *J. Chem. Soc., Dalton Trans.* **1995**, 83–97.

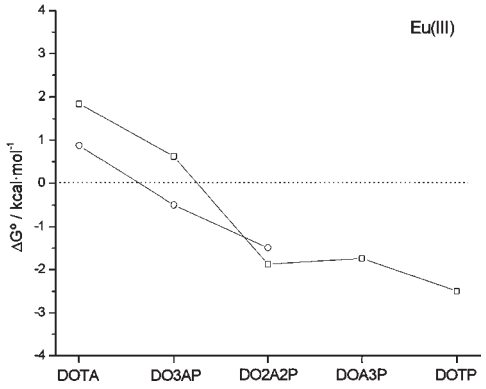

Figure 4. Experimental (○) and calculated (□) relative free energies for the SAP ⇆ TSAP equilibrium of Eu^{3+} complexes. Positive relative free energies indicate that the SAP isomer is more stable than the TSAP one.

Relative Energies of the TSAP and SAP Isomers. The relative populations of the TSAP and SAP conformations of lanthanide complexes of DOTA[5] and DO3AP[13] have been studied in detail by using NMR spectroscopy. One can easily derive the relative free energies from the populations of the two isomers using the formula $\Delta G^\circ = -RT \ln K$. The relative energies of these isomers in $[Eu(DO2A2P)]^{3-}$ have been also investigated.[16] The experimental relative free energies available in the literature for the Eu^{3+} complexes of DOTA, DO3AP, and DO2A2P are shown in Figure 4. The experimental evidence indicates that the TSAP geometry is progressively stabilized upon replacement of the acetate arms of DOTA by methylenephosphonate groups. In the case of the $[Eu(DOTA)(H_2O)]^-$ complex, the SAP conformation is the most abundant one in solution (ca. 80%), while for the $[Eu(DO2A2P)]^{3-}$ complex, the SAP abundance amounts only to ca. 7%.[16] Ln(DOTP) complexes are known to exist as the TSAP isomer both in the solid state and in solution.[12]

To understand the reasons for the stabilization of the TSAP isomer upon an increase in the number of methylenephosphonate pendants in Ln^{3+}(DOTA)-like complexes, we have calculated the relative free energies of the SAP and TSAP conformations for the $[Eu(L)(H_2O)_q]^{n-}$ systems [L = DOTA, $q = 1$, $n = 1$; L = DO3AP, $q = 1$, $n = 2$; L = DO2A2P, $q = 0$, $n = 3$; L = DOA3P, $q = 0$, $n = 4$; L = DOTP, $q = 0$, $n = 5$]. Furthermore, we have also calculated the relative free energies for the corresponding eight-coordinate $[Lu(L)]^{n-}$ systems. The energetic trend predicted by our calculations agrees well with the experimental one (Figure 4; see also Table 4). Furthermore, calculated relative free energies are in reasonably good quantitative agreement with the experimental values, with a somewhat larger deviation being observed for the $[Eu(DO3AP)]^{2-}$ complex (ca. 1.1 kcal·mol^{-1}). The counterpoise-corrected relative BEs of the macrocyclic ligand in the different octacoordinated Lu^{3+} complexes are given in Table 4. Our calculations provide negative relative BEs, calculated as $BE = BE_{TSAP} - BE_{SAP}$. The actual BEs are positive, and thus a negative relative BE indicates that the SAP conformation of the ligand provides a stronger binding to the lanthanide ion for all complexes investigated. This is attributed to a stronger binding of the lanthanide to the donor atoms of the macrocycle in the SAP geometry when compared to the TSAP one (Table 2). The relative SEs of the ligand ($SE = SE_{TSAP} - SE_{SAP}$) are all negative; the ligand energies, as well as the complex energies, are negative, and therefore a negative relative SE indicates a higher degree of steric strain in the SAP form with respect to the TSAP one. The replacement of acetate groups of DOTA by bulkier methylenephosphonate pendant arms further increases the steric strain in the SAP form with respect to the TSAP one. This increased steric strain is not fully compensated for by the increased BE obtained upon introduction of methylenephosphonate pendants in the SAP form. Thus, the introduction of methyphosphonate pendant arms in DOTA-like systems stabilizes the TSAP isomer as a result of the high steric demand of the phosphonate groups, and the higher strain of the ligand in the SAP isomer. The successive substitution of acetate arms with methylphosphonate groups must introduce, in addition to steric effects, significant electrostatic repulsive effects due to the higher negative charge of the phosphonate groups. However, according to our calculations the SAP geometry does not force the phosphonate groups to be closer than the TSAP conformation. For instance, the distances between the phosphorus atoms of neighboring pendant arms in the SAP and TSAP isomers of $[Eu(DOTP)]^{5-}$ are identical (5.20 Å).

Table 4. Relative Free Energies (ΔG°) for the SAP ⇆ TSAP Equilibrium, Relative BEs, Relative SEs of the Ligands, and Relative BSSEs (kcal·mol^{-1})

Ln		DOTA	DO3AP	DO2A2P	DOA3P	DOTP
Eu	ΔG°_{exptl}	0.87	−0.42	−1.49	c	d
	ΔG°_{calcd} [a]	1.84	0.62	−1.87	−1.74	−2.50
Lu	ΔG°_{exptl}	1.00	0.82	d	c	d
	ΔG°_{calcd} [a]	2.10	0.62	−0.82	−1.24	−2.58
	BE[b]	−3.63	−4.08	−4.81		−9.04
	SE[a]	−0.85	−3.02	−5.93		−10.50
	BSSE[b]	0.29	−0.50	−0.31		−0.72

[a] Relative free energies are defined as $\Delta G^\circ = G^\circ_{TSAP} - G^\circ_{SAP}$. Note that the actual values of the complex free energies are negative, and therefore a positive relative free energy indicates that the SAP isomer is more stable than the TSAP one. The same holds for the relative SEs because the actual ligand energies are negative. [b] The actual values of the BSSEs and BEs are positive, so that a negative energy indicates that the respective BSSE or BE is greater for the SAP isomer. [c] Data not available. [d] The complexes exist in solution only as the TSAP isomer.

NMR studies have shown that the abundance of the TSAP isomer is progressively decreasing, moving to the right across the lanthanide series.[5,13] To understand the reasons for this trend, we have calculated the relative free energies of the SAP and TSAP isomers of the $[Ln(DO3AP)(H_2O)]^{2-}$ complexes. The results are compared to the experimental ones in Figure 5 (see also Table 5). Our calculations indeed predict a stabilization of the SAP isomer upon an increase in the atomic number of the lanthanide ion, in nice agreement with the experimental results. Furthermore, the quantitative agreement between the experimental and calculated values is also reasonably good, in particular for the heaviest lanthanide ions. The TSAP isomer is predicted to be the most stable one for the large lanthanides (La−Nd), while for the heaviest lanthanides, the SAP form becomes the most stable one. The experimental data show a very similar trend, although the TSAP form is the most abundant one for a larger number of lanthanides (La−Gd). Inclusion of

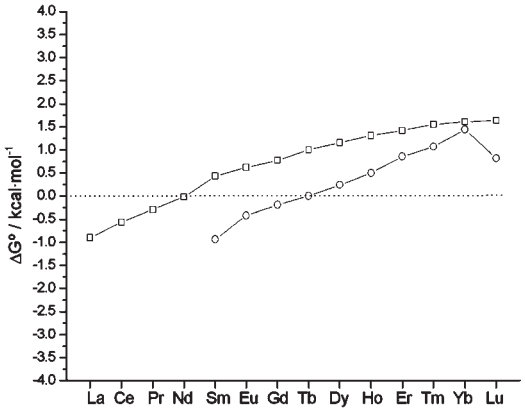

Figure 5. Experimental (○) and calculated (□) relative free energies for the SAP ⇆ TSAP equilibrium in $[Ln(DO3AP)(H_2O)]^{2-}$ complexes.

Table 5. Relative Free Energies ($\Delta G°$) for the SAP ⇆ TSAP Equilibrium in $[Ln(DO3AP)(H_2O)]^{2-}$ Complexes, Relative BEs, Relative SEs of the Ligands, and Relative BSSEs (kcal·mol^{-1})

Ln	$\Delta G°_{exptl}$	$\Delta G°_{calcd}$[a]	BE[b]	SE[a]	BSSE[b]
La	c	−0.90	−2.53	−2.70	−0.84
Ce	c	−0.56	−2.62	−2.52	−0.92
Nd	c	−0.02	−3.29	−2.69	−0.74
Eu	−0.42	0.62	−4.26	−3.07	−0.57
Ho	0.50	1.31	−4.66	−3.07	−0.71
Tm	1.07	1.55	−5.88	−3.85	−0.09
Lu	0.82	1.64	−6.85	−4.39	0.32

[a] Relative free energies are defined as $\Delta G° = G°_{TSAP} - G°_{SAP}$. Note that the actual values of the complex free energies are negative, and therefore a positive relative free energy indicates that the SAP isomer is more stable than the TSAP one. The same holds for the relative SEs, as the actual ligand energies are negative. [b] The actual values of the BSSEs and BEs are positive, so that a negative energy indicates that the respective BSSE or BE is greater for the SAP isomer. [c] The complexes exist in solution only as the TSAP isomer.

solvent effects (water) by using the PCM model provokes a stabilization of the TSAP isomer with respect to the SAP one by ∼2.0−3.1 kcal·mol^{-1}. However, solvent inclusion does not substantially affect the trend observed for the relative energies along the lanthanide series. A stabilization of the TSAP isomer with respect to the SAP one upon inclusion of solvent effects was previously observed for the $[Ln(DOTA)(H_2O)]^-$ complexes. This was attributed to the different polarities of the two isomers: the TSAP isomer is more polar and, consequently, is more stabilized by polar solvents.[21]

Table 5 shows the relative BEs and relative SEs of the SAP and TSAP isomers calculated for different $[Ln(DO3AP)(H_2O)]^{2-}$ complexes. Our results indicate that the relative SE of the SAP form is only slightly increased as the ionic radius of the lanthanide ion decreases (ca. 1.7 kcal·mol^{-1} from La to Lu), which can be attributed to the more compact structure of the complexes with the smaller lanthanide ions. The relative BEs, however, experience an important change along the lanthanide series. The SAP form provides the stronger interaction between the ligand and the lanthanide ion along the whole lanthanide series. This effect is magnified as the ionic radius of the lanthanide ion decreases, with the relative BEs changing from ca. −2.5 to −6.8 kcal·mol^{-1} from La to Lu. Thus, the SAP isomer appears to be endowed with the highest BE, which also

Scheme 1. Inversion of a Five-Membered Chelate Ring Formed upon Coordination of the Macrocyclic Fragment of the Ligand

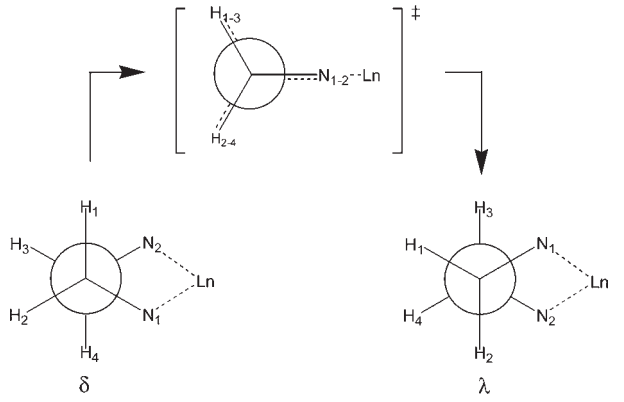

increases with respect to that of the TSAP isomer across the lanthanide series as the charge density of the metal ion increases.

TSAP ↔ SAP Interconversion Process. The interconversion between the TSAP and SAP isomers has been investigated experimentally for several $[Ln(DOTA)(H_2O)]^-$ complexes[7,8] and for the $[Ln(DO2A2P)]^{3-}$ ones (see above). These studies have concluded that the SAP ↔ TSAP interconversion process may proceed following two different pathways: (i) the inversion of the five-membered chelate rings formed upon coordination of the cyclen moiety, which leads to a ($\delta\delta\delta\delta$) ↔ ($\lambda\lambda\lambda\lambda$) conformational change; (ii) the rotation of the pendant arms, which results in a $\Delta \leftrightarrow \Lambda$ configurational change. The TSAP ↔ SAP interconversion process has been also investigated by using ab initio calculations on the $[Lu(DOTA)]^-$ system.[21] Aiming to obtain a deeper understanding of the dynamic processes occurring in this family of complexes, we have performed a detailed investigation of the arm rotation and cyclen inversion path in the $[Lu(DO2A2P)]^{3-}$ system.

According to our results obtained on B3LYP/6-31G*-optimized geometries, the inversion of the cyclen moiety in the $[Lu(DO2A2P)]^{3-}$ complex is a four-step process. In each of these steps, one five-membered chelate ring changes its configuration from δ to λ, passing through a transition state (TS) in which the chelate ring adopts a nearly planar conformation with the NCCN moiety in an eclipsed disposition (Scheme 1). Attempts to search for a concerted path in which the four chelate rings change their configuration simultaneously were unsuccessful. The optimized geometry of the TSAP conformation of the $[Lu(DO2A2P)]^{3-}$ complex [$\Delta(\delta\delta\delta\delta)$ form] shows a nearly undistorted C_2 symmetry, with the symmetry axis containing the metal ion and being perpendicular to the plane described by the four nitrogen atoms of the cyclen moiety. Because of the symmetry properties of the molecule, there are two different types of five-membered chelate rings formed as a result of coordination of the cyclen moiety. These different five-membered chelate rings are labeled with subscripts "a" and "b" in Table 6. Thus, the TSAP conformation of the $[Lu(DO2A2P)]^{3-}$ complex is labeled as $\Delta(\delta_{1a}\delta_{1b}\delta_{2a}\delta_{2b})$, where the five-membered chelate rings labeled as "a" lie below an acetate pendant arm and those labeled as "b" are placed below a methylenephosphonate group (Figure 1). The inversion

Table 6. Relative Free Energies of Minima, Intermediates (I), and Transition States (TS) Involved in the TSAP ↔ SAP Interconversion Process of $[Ln(DO2A2P)]^{3-}$ (Ln = La or Lu) Complexes (kcal·mol^{-1}).[a]

		inversion			rotation
	ring	Lu	La	arm	Lu
TSAP	$\Delta(\delta_{1a}\delta_{1b}\delta_{2a}\delta_{2b})$	0.00	0.00	TSAP	0.00
$TS_{TSAP-1a}$	$\Delta(\delta_{1a}\delta_{1b}X_{2a}\delta_{2b})$	13.50	15.38	TS_1	19.34
$TS_{TSAP-1b}$	$\Delta(\delta_{1a}X_{1b}\delta_{2a}\delta_{2b})$	13.50		I_1	15.78
I_{1a}	$\Delta(\delta_{1a}\delta_{1b}\lambda_{2a}\delta_{2b})$	4.29	5.76	TS_2	18.84
I_{1b}	$\Delta(\delta_{1a}\lambda_{1b}\delta_{2a}\delta_{2b})$	6.47		I_2	17.58
TS_{1a-2a}	$\Delta(X_{1a}\delta_{1b}\lambda_{2a}\delta_{2b})$	12.48	15.35	TS_3	22.32
TS_{1b-2b}	$\Delta(\delta_{1a}\lambda_{1b}\delta_{2a}X_{2b})$	14.08		I_3	18.25
TS_{1a-2c}	$\Delta(\delta_{1a}X_{1b}\lambda_{2a}\delta_{2b})$	14.71		TS_4	19.36
TS_{1b-2d}	$\Delta(X_{1a}\lambda_{1b}\delta_{2a}\delta_{2b})$	16.26		SAP	0.82
TS_{1a-2d}	$\Delta(\delta_{1a}\delta_{1b}\lambda_{2a}X_{2b})$	17.18			
TS_{1b-2c}	$\Delta(\delta_{1a}\lambda_{1b}X_{2a}\delta_{2b})$	18.79			
I_{2a}	$\Delta(\lambda_{1a}\delta_{1b}\lambda_{2a}\delta_{2b})$	3.03	5.17		
I_{2b}	$\Delta(\delta_{1a}\lambda_{1b}\delta_{2a}\lambda_{2b})$	7.09			
I_{2c}	$\Delta(\delta_{1a}\lambda_{1b}\lambda_{2a}\delta_{2b})$	7.87			
I_{2d}	$\Delta(\delta_{1a}\delta_{1b}\lambda_{2a}\lambda_{2b})$	8.98			
TS_{2a-3a}	$\Delta(\lambda_{1a}\delta_{1b}\lambda_{2a}X_{2b})$	12.48	14.36		
TS_{2c-3a}	$\Delta(\delta_{1a}\lambda_{1b}X_{2a}\delta_{2b})$	15.23			
TS_{2d-3b}	$\Delta(\delta_{1a}X_{1b}\lambda_{2a}\lambda_{2b})$	16.88			
TS_{2c-3b}	$\Delta(\delta_{1a}\lambda_{1b}\lambda_{2a}X_{2b})$	17.17			
TS_{2d-3a}	$\Delta(X_{1a}\delta_{1b}\lambda_{2a}\lambda_{2b})$	17.51			
TS_{2b-3b}	$\Delta(\delta_{1a}\lambda_{1b}X_{2a}\lambda_{2b})$	18.07			
I_{3a}	$\Delta(\lambda_{1a}\delta_{1b}\lambda_{2a}\lambda_{2b})$	3.55	6.50		
I_{3b}	$\Delta(\delta_{1a}\lambda_{1b}\lambda_{2a}\lambda_{2b})$	7.76			
TS_{3a-SAP}	$\Delta(\lambda_{1a}X_{1b}\lambda_{2a}\lambda_{2b})$	12.52	15.07		
TS_{3b-SAP}	$\Delta(X_{1a}\lambda_{1b}\lambda_{2a}\lambda_{2b})$	17.24			
SAP	$\Delta(\lambda_{1a}\lambda_{1b}\lambda_{2a}\lambda_{2b})$	0.82	3.19		

[a] A nearly planar conformation with the NCCN moiety in an eclipsed disposition is denoted as X.

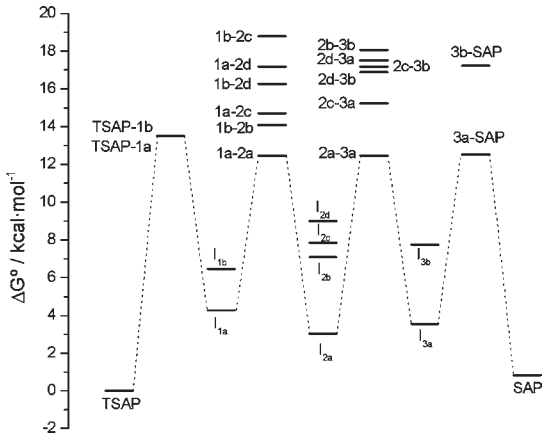

Figure 6. In vacuo relative free energies of minima, intermediates, and transition states involved in the ring-inversion process of $[Lu(DO2A2P)]^{3-}$.

of the cyclen moiety may therefore proceed either through the inversion of an "a" chelate ring, leading to a $\Delta(\delta_{1a}\delta_{1b}\lambda_{2a}\delta_{2b})$ intermediate (I_{1a}) or through the inversion of a "b" chelate ring, resulting in the formation of a $\Delta(\delta_{1a}\lambda_{1b}\delta_{2a}\delta_{2b})$ intermediate (I_{1b}; Figure 6). The TSAP conformation and intermediates I_{1a} and I_{1b} are related by transition states $TS_{TSAP-1a}$ and $TS_{TSAP-1b}$, respectively. The activation free energies calculated for the formation of I_{1a} and I_{1b} are virtually identical, while I_{1a} is more stable than I_{1b} by ca. 2.2 kcal·mol^{-1}. In both the I_{1a} and I_{1b} forms, there are three chelate rings with the δ configuration that can be inverted; symmetry considerations indicate that there are only four new intermediates that

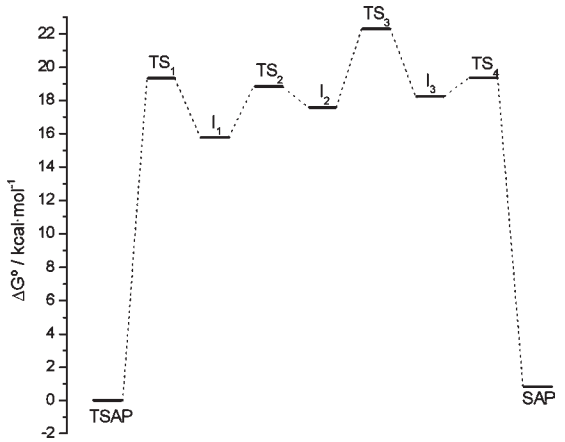

Figure 7. In vacuo relative free energies of minima, intermediates, and transition states involved in the arm-rotation process of $[Lu(DO2A2P)]^{3-}$.

can be formed upon inversion of a second chelate ring, which are labeled as I_{2a}, I_{2b}, I_{2c}, and I_{2d} (Figure 6). However, there are up to six transition states connecting I_{1a} and I_{1b} with these intermediates. This is due to the fact that I_{2c} and I_{2d} can be generated from both I_{1a} and I_{1b} through two different transition states. For instance, I_{2c} $[\Delta(\delta_{1a}\lambda_{1b}\lambda_{2a}\delta_{2b})]$ can be generated by inversion of an ethylenediamine unit of both I_{1a} and I_{1b} (Table 6). Among intermediates I_{2a}, I_{2b}, I_{2c}, and I_{2d}, those showing C_2 symmetry (I_{2a} and I_{2b}) present a lower energy than those with C_1 symmetry (I_{2c} and I_{2d}). Inspection of the calculated geometries of I_{2a} and I_{2b} shows that the lowest energy of I_{2a} can be attributed to the lower steric hindrance generated by the bulky phosphonate groups. Inversion of a third chelate ring leads to the formation of intermediates I_{3a} and I_{3b}, but again there are up to six transition states relating the latter with I_{2a}, I_{2b}, I_{2c}, and I_{2d}. The lowest-energy pathway appears to be the transformation of I_{2a} into I_{3a} (Figure 6). Finally, intermediates I_{3a} and I_{3b} convert to the SAP form of the complex through inversion of the fourth ethylenediamine unit.

For the La^{3+} complex we did not perform the detailed investigation of the ring-inversion process carried out for the Lu^{3+} analogue. Instead, only those geometries of intermediates and transition states providing the lowest energy path for Lu^{3+} have been optimized. Our results provide slightly higher free energy barriers for the La^{3+} complex than for the Lu^{3+} one (Table 6). Assuming the rate determining step to be the passage between TSAP and the first intermediate, I_{1a}, the barrier for the ring inversion path is the one associated to $TS_{TSAP-1a}$, which amounts to 13.5 and 15.4 kcal·mol^{-1} for the Lu^{3+} and La^{3+} complexes, respectively. These values are in excellent agreement with the experimental values obtained from the analysis of the NMR spectra (15.4 and 15.7 kcal·mol^{-1} for Lu and La complexes, respectively).[16]

Our calculations on the $[Lu(DO2A2P)]^{3-}$ system indicate that the arm-rotation process responsible for the TSAP ↔ SAP interconversion is also a four-step process involving the stepwise rotation of each of the four pendant arms of the DO2A2P ligand (Figure 7). Indeed, the rotation of one of the phosphonate groups of the TSAP form leads to the formation of intermediate I_1. In this process, the NCPO dihedral angle changes from −50.5° in

the TSAP form to 42.3° in I_1, passing through a nearly planar disposition in the transition state (TS_1, 11.7°). Several attempts to search for an intermediate in which one of the acetate arms is rotated with respect to the remaining three pendant arms of the ligand have been failed. Subsequent rotation of the two acetate pendants provides intermediates I_2 and I_3 through transition states TS_2 and TS_3, respectively. In these transition states, the NCCO dihedrals amount to −11.6 and 10.0°, respectively. Finally, rotation of the second methylenephosphonate pendant gives the SAP form of the complex through transition state TS_4 (Figure 7).

Assuming that the rate-determining step for the rotation of the pendant arms is the one associated with the passage from TSAP to I_1, we estimate a free-energy barrier of 19.3 kcal·mol^{-1} for the rotation processes of [Lu(DO2A2P)]$^{3-}$. This values compares reasonably well with that obtained experimentally (15.8 kcal·mol^{-1}). We want to highlight that our geometry optimizations of energy minima and transition states, performed in vacuo, did not take into account the possible influence of the solvent in the mechanism of the process. However, the calculated free-energy barriers for both the arm-rotation and ring-inversion processes compare reasonably well with the experimental values, which supports that the mechanism predicted by our calculations is basically correct. Furthermore, a similar agreement is observed when comparing the experimental and calculated $\Delta H^{\ddagger}$ values, which are expected to be less sensitive to solvent reorganization processes. Moreover, solvated single-point energy calculations performed at all critical points along both interconversion pathways show that the inclusion of solvent effects (water) provokes only a small variation in the calculated free-energy barriers (< 3 kcal·mol^{-1}).

Cosentino et al.[21] reported a computational investigation of the SAP ↔ TSAP interconversion process in [LuDOTA)]$^-$. Their results on in vacuo HF/3-21G-optimized geometries indicated that the arm rotation is a single-step process involving the simultaneous rotation of the four acetate arms. In the case of the [Lu(DO2A2P)]$^{3-}$ system, our attempts to search for a single-step path have not provided any results. Thus, we have reexamined the arm-rotation process in [Lu(DOTA)]$^-$ at the B3LYP/6-31G* level. Our results confirm those obtained previously at the HF/3-21G level. Indeed, according to our calculations, the arm rotation in [Lu(DOTA)]$^-$ is a one-step process involving the simultaneous rotation of the four pendants. The free-energy barrier calculated for the arm-rotation process responsible for the SAP ↔ TSAP interconversion process in [Lu(DOTA)]$^-$ amounts to 19.6 kcal·mol^{-1} (Table 7). This value is only somewhat higher than the experimental one obtained for the [Yb(DOTA)]$^-$ complex (15.6 kcal·mol^{-1}).[7] Although we do not have a definitive explanation for the different mechanisms responsible for the arm-rotation process in [Lu(DOTA)]$^-$ and [Lu(DO2A2P)]$^{3-}$ complexes, we believe that the higher symmetry of the [Lu(DOTA)]$^-$ complex (C_4) in comparison with the [Lu(DO2A2P)]$^{3-}$ one (C_2) could stabilize a concerted rotation of the four pendant arms. An alternative explanation could be that the tetrahedral arrangement of the phosphonate groups in DO2A2P hinders the transition state of the concerted mechanism because of steric crowding, while the planar arrangement of the acetate groups of DOTA favors a concerted mechanism.

Table 7. Relative Free Energies of Minima, Intermediates (I), and Transition States (TS) Involved in the SAP ↔ TSAP Interconversion Process of [Lu(DOTA)]$^-$ (kcal·mol^{-1})[a]

	ring inversion		arm rotation	
SAP	Δ(λλλλ)	0.00	A	0.00
TS_{SAP-1}	Δ(Xδδδ)	13.93	$TS_{SAP-TSAP}$	19.60
I_1	Δ(δλλλ)	5.72	IA	2.10
TS_{1-2a}	Δ(δλXλ)	15.36		
TS_{1-2b}	Δ(δXλλ)	16.30		
I_{2a}	Δ(δλδλ)	6.17		
I_{2b}	Δ(δδλλ)	9.14		
TS_{2a-I3}	Δ(δXδλ)	14.17		
TS_{2b-I3}	Δ(δδXλ)	16.17		
I_3	Δ(δδδλ)	6.80		
TS_{3-TSAP}	Δ(δδδX)	15.05		
TSAP	Δ(δδδδ)	2.10		

[a] A nearly planar conformation with the NCCN moiety in an eclipsed disposition is denoted as X.

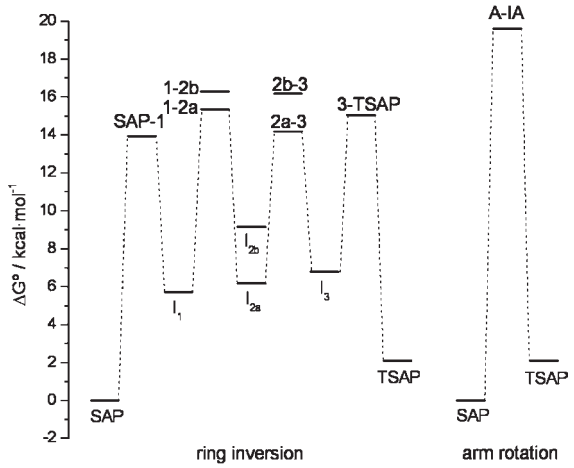

Figure 8. In vacuo relative free energies of minima, intermediates, and transition states involved in the ring-inversion and arm-rotation processes of [Lu(DOTA)]$^-$.

A detailed investigation of the ring-inversion process in the [Lu(DOTA)]$^-$ system provides an interconversion pathway similar to that obtained for the DO2A2P analogue. However, the higher symmetry of the molecule reduces the number of possible intermediates and transition states along the interconversion path. Our results are summarized in Table 7 and Figure 8. Again, among the two possible interconversion pathways, the lowest-energy one is that providing an intermediate with C_2 symmetry (I_{2a}). Assuming that the rate-determining step for the inversion of the macrocyclic ring is the one associated with the passage from I_1 to I_{2a}, we estimate a free-energy barrier of 15.4 kcal·mol^{-1}. This value is in excellent agreement with those obtained experimentally for the [Yb(DOTA)]$^-$ (14.6 kcal·mol^{-1})[7] and [Lu(DOTA)]$^-$ (15.8 kcal·mol^{-1})[8] complexes.

Calculation of ^{13}C NMR Shifts. In previous works, we have demonstrated that quantum-mechanical GIAO calculations of ^{13}C NMR chemical shifts can be used as a tool for the structure validation of coordination compounds.[51] It has been shown experimentally that the [Ln(DO2A2P)]$^{3-}$

(51) (a) Platas-Iglesias, C.; Esteban, D.; Ojea, V.; Avecilla, F.; de Blas, A.; Rodríguez-Blas, T. *Inorg. Chem.* **2003**, *42*, 4299–4307. (b) Vaiana, L.; Regueiro-Figueroa, M.; Mato-Iglesias, M.; Platas-Iglesias, C.; Esteban-Gómez, D.; de Blas, A.; Rodríguez-Blas, T. *Inorg. Chem.* **2007**, *46*, 8271–8282.

Table 8. Experimental ^{13}C NMR Shifts (ppm) for the $[Ln(DO2A2P)]^{3-}$ Complexes (Ln = La or Lu) and Calculated (GIAO Method) ^{13}C NMR Chemical Shift Values for the SAP and TSAP Isomers[a]

	Lu			La		
		calcd			calcd	
	exptl[a]	SAP	TSAP	exptl[b]	SAP	TSAP
NCCO	180.3	189.7	187.8	180.4	180.7	176.9
NCCO	59.9	72.2	68.8	60.7	74.8	71.9
NCPO	53.9	72.2	58.5	54.4	75.9	64.1
CNCCO	53.7	55.2	53.6	53.7	62.0	58.2
CNCPO	52.0	61.4	53.4	52.1	66.1	61.7
CNCPO	51.6	54.7	50.8	51.9	60.2	56.7
CNCCO	48.8	55.1	49.6	49.5	61.3	56.7
AF_i[c]		0.120	0.057		0.151	0.092

[a] Reference 16. [b] This work. [c] $AF_i = [\sum(\text{exp} - \text{calcd})^2/\sum(\text{exp})^2]^{1/2}$, where exp and calcd denote calculated and experimental values, respectively.

complexes (Ln = La, Lu) exist in solution mainly as the TSAP isomer (see above). To validate the experimental assignments, the ^{13}C NMR shielding constants of the SAP and TSAP forms of the $[Ln(DO2A2P)]^{3-}$ complexes (Ln = La or Lu) were calculated by using the GIAO method. It has been reported that calculation of the NMR shielding constants using the 46 + $4f^{14}$ core electron of Dolg et al.[29] provides inconsistent ^{13}C NMR chemical shifts.[21] Therefore, in these calculations, we used the 46-core-electron ECPs by Stevens et al.,[41,42] which were shown to provide ^{13}C NMR chemical shifts close to the experimental values.[21]

The calculated ^{13}C NMR shifts for the two isomers are compared in Table 8 with the experimental values obtained for the major conformation observed in solution, which has been assigned to the TSAP form. The ^{13}C NMR shifts calculated for the TSAP conformation at the B3LYP/6-311G** level provide a much better agreement with the experimental values than those obtained for the SAP form, as evidenced by the agreement factors obtained (AF_i; Table 8). The better agreement between the experimental shifts and those calculated for the TSAP conformation is clearly confirmed by Figure 9, which shows the differences between experimental and theoretical ^{13}C NMR shift values ($\Delta\delta$)[52] for the SAP and TSAP isomers of $[Ln(DO2A2P)]^{3-}$ (Ln = La or Lu). There are obviously larger deviations from the experimental values for all carbon nuclei of the SAP form than for the same nuclei in the TSAP one (with the exception of the carbonyl resonance in the La^{3+} complex). These results therefore confirm that the major isomer observed in solution for the $[Ln(DO2A2P)]^{3-}$ complexes corresponds to the TSAP conformation, in agreement with the relative free energies of the two isomers discussed above. These results also confirm that DFT calculations, in combination with the GIAO approach, can be used for structure validation of DOTA-like complexes in solution. However, we notice that the agreement between the experimental and calculated theoretical shifts is considerably better for the Lu^{3+} complex than for the La^{3+} one. This result suggests that the calculated structure of the Lu^{3+} complex is closer to its actual solution structure than that of La^{3+}. This could be related to the presence in solution of an inner-sphere water molecule coordinated to the large La^{3+} ion, but further experimental data are required to clarify this point.

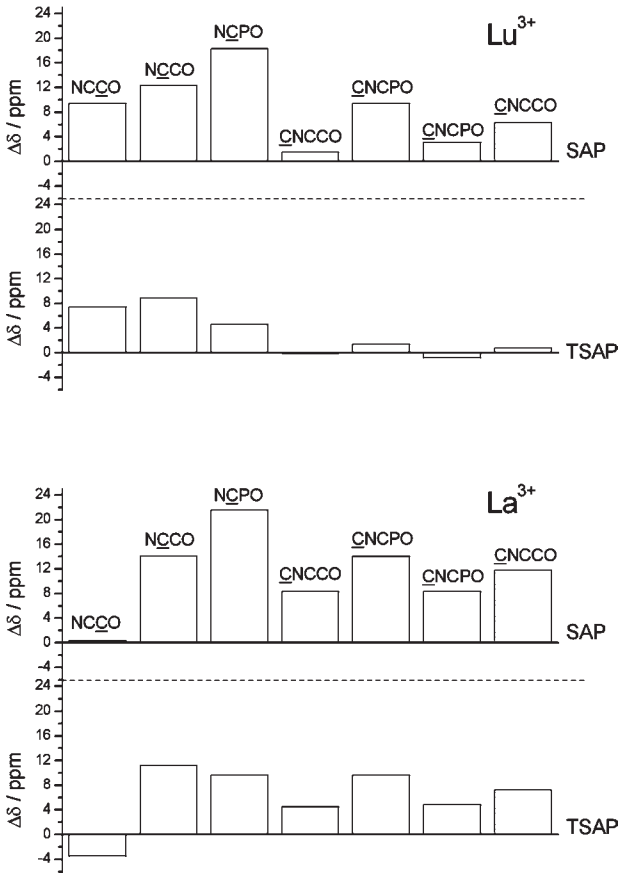

Figure 9. Differences between experimental and theoretical ^{13}C NMR chemical shifts (B3LYP/6-311G** level) for the SAP and TSAP conformations of $[Ln(DO2A2P)]^{3-}$ complexes (Ln = La or Lu).

Conclusions

Theoretical calculations performed at the DFT (B3LYP) level are able to capture several properties of Ln^{3+}(DOTA) analogues containing methylenephosphonate pendant arms. These properties include (i) the stabilization of the TSAP conformation upon an increase in the number of methylenephosphonate groups in the ligand, (ii) the stabilization of the SAP form upon proceeding to the right across the lanthanide series, (iii) the TSAP enantiomerization process, and (iv) the ^{13}C NMR spectra. According to our calculations, the introduction of methyphosphonate pendant arms in DOTA-like systems stabilizes the TSAP isomer as a result of the high steric demand of the phosphonate groups and the higher strain of the ligand in the SAP isomer. The SAP conformation of the ligand provides the highest BE to the metal ion, which further increases with respect to that of the TSAP form across the lanthanide series as the charge density of the metal ion increases. The calculations presented in this paper confirm that the enantiomerization process requires both inversion of the five-membered rings formed upon coordination of the macrocyclic moiety and rotation of the pendant arms. These two consecutive processes result in the overall conversion of the enentiomeric pairs [TSAP $\Delta(\delta\delta\delta\delta)$ and TSAP $\Lambda(\lambda\lambda\lambda\lambda)$] of the dominating TSAP isomer. According to our B3LYP/6-31G(d) results, the arm-rotation pathway in

(52) Barone, G.; Gomez-Paloma, L.; Duca, D.; Silvestri, A.; Riccio, R.; Bifulco, G. *Chem.—Eur. J.* **2002**, *8*, 3233–3239.

$[Lu(DOTA)]^-$ is a single-step process, while for $[Lu(DO2A2P)]^{3-}$, it is a multistep path involving the stepwise rotation of each of the four pendant arms. Finally, our results show that DFT calculations, in combination with the GIAO approach, can be used for the structure validation of DOTA-like complexes in solution.

Acknowledgment. This research was supported, in part, by grants from OTKA K 69098 and OTKA K63388. C. P.-I., A.d.B., and T.R.-B. thank the Ministerio de Educación y Ciencia and FEDER (Grant CTQ2006-07875/PPQ) and Xunta de Galicia (Grant INCITE08-ENA103005ES) for financial support. This research was performed in the framework of the EU COST Action D38 "Metal-Based Systems for Molecular Imaging Applications". The authors are indebted to Centro de Supercomputación de Galicia (CESGA) for providing the computer facilities. We thank Dr. Zoltán Kovács for a generous gift of DO2A2P.

Supporting Information Available: ^1H, ^{13}C, ^{31}P, 2D COSY, EXSY, and HSQC NMR spectra of $[La(DO2A2P)]^{3-}$, ^1H NMR spectral data for $[La(DO2A2P)]^{3-}$, in vacuo optimized Cartesian coordinates for the TSAP and SAP conformations of $[Ln(DOTA)(H_2O)]^-$, $[Ln(DO3AP)(H_2O)]^{2-}$, $[Ln(HDO3AP)(H_2O)]^-$, $[Ln(DO2A2P)]^{3-}$, $[Ln(DOA3P)]^{4-}$, and $[Ln(DOTP)]^{5-}$ complexes, and optimized Cartesian coordinates for the intermediates and transition states involved in the ring-inversion and arm-rotation processes of $[Lu(DOTA)]^-$, $[La(DO2A2P)]^{3-}$, and $[Lu(DO2A2P)]^{3-}$ complexes. This material is available free of charge via the Internet at http://pubs.acs.org.